The Astrophysical Journal, 468:L103–L106, 1996 September 10

HUBBLE SPACE TELESCOPE OBSERVATIONS OF JETS FROM YOUNG STARS

Thomas P. Ray
School of Cosmic Physics, Dublin Institute for Advanced Studies, 5 Merrion Square, Dublin 2, Ireland
Reinhard Mundt
Max-Planck-Institut für Astronomie, 69117 Heidelberg, Germany
John E. Dyson
Department of Physics and Astronomy, University of Leeds, Leeds LS2 9JT, England
Sam A. E. G. Falle
Department of Applied Mathematical Studies, University of Leeds, Leeds LS2 9JT, England
and
Alejandro C. Raga
Instituto de Astronomía, Universidad Nacional Autonoma de México, Apartado Postal 70-264, México, DF 04510
Received 1996 April 30; accepted 1996 June 21

ABSTRACT

We report on *Hubble Space Telescope* (*HST*) emission line ([S II]λλ6716,6731, Hα, and [O I]λ6300) and nearby continuum imaging of the HL Tau and HH 30 jets from our own *HST* program as well as a study of *HST* Archive [S II]λλ6716,6731 images of the HH 1 and HH 34 jets. It is found in all cases that these jets are well resolved in the lateral direction (with FWHM diameters ≳0.″2) as far as we can follow them to their source which, in the case of HH 30, is as close as 0.″25 (35 AU). Assuming the jet has essentially zero angular width at its origin, one can deduce a *lower bound* for the initial opening angle, and the values obtained are very large indeed (e.g., ≳60° for the HH 30 jet and counterjet). Our data are shown to support models in which the jet is initially poorly focused before being asymptotically collimated into a "column" with a diameter of order a few tens of AU. As regards the origin of the knots seen in these jets, it is found that many of the knots in the HH 1 and HH 34 jets resemble internal bow shocks, at least far away from their driving source (≳5″ and 10″ in the case of HH 1 and HH 34 jets, respectively). This is consistent with models in which the knots are attributed to "internal working surfaces" caused by temporal variations in the outflow from the source. It is found in the case of the HH 30 jet, however, that its knots, at least close to the source, might have another origin.

Subject headings: ISM: jets and outflows — stars: formation — stars: mass loss

1. INTRODUCTION

Herbig-Haro (HH) jets (see, e.g., Edwards, Ray, & Mundt 1993) are perhaps the most dramatic illustrations of the outflow phenomenon seen in the case of young stars. They are highly supersonic, with Mach numbers greater than about 20, and are very well collimated, at least several hundred AU from their source. Often they consist of a series of quasi-periodically spaced knots, and their total length can vary from a few hundred AU to several tenths of a parsec. The origin of the knots is uncertain although it is clear that their emission derives from shocks. Models for their formation include the idea that they are due to the growth of hydrodynamic instabilities (Bodo et al. 1994) and that they are "internal working-surfaces" caused by variations in the supersonic outflow from the source (e.g., Raga 1995). One test of such models is to examine the detailed morphology of the knots themselves: e.g., the "internal working-surfaces" hypothesis predicts that the knots should look like small bow shocks (Raga 1995), whereas if they are caused by hydrodynamic instabilities, they may look like oblique crossing-shocks (Bodo et al. 1994). Unfortunately the typical angular diameter of these knots (≲1″) precludes such detailed studies, at least from the ground.

Some years ago evidence was found from ground-based data that the angular diameter D of a HH jet often appeared to decrease more slowly than L, where L is the angular distance to the source (Mundt, Ray, & Raga 1991; Raga, Mundt, & Ray 1991). Defining the local "opening" angle θ of the jet as D/L, θ was thus found to increase as L became smaller. While the limiting resolution of ground-based optical telescopes meant that it was not possible to confirm this trend closer to the source than usually a few arcseconds; nevertheless it was clear from the data of Mundt et al. (1991) that the rise in local opening angle was dramatic. For example in some cases the angular width of the first measurable knot, as seen from the source, was of the order of 20°–30°. Obviously, determining the degree of jet collimation in the vicinity of the source is of fundamental importance to understanding how young stellar object (YSO) jets propagate and could give us vital clues as to how they are formed.

With these aims in mind we undertook a study, on which we report in this Letter, of several HH jets based on a *HST* program of our own (for the HL Tau and HH 30 jets) and the *HST* Archive (for the HH 1 and HH 34 jets). For background details on individual jets the reader is referred to Mundt, Ray, & Bührke (1988) and Mundt et al. (1990) (hereafter MRBRS) for the neighbouring HL Tau and HH 30 outflows, to Eislöffel, Mundt, & Böhm (1994) for HH 1, and to Bührke, Mundt, & Ray (1988) and Eislöffel & Mundt (1992) for HH 34. The implications of our findings in connection with the collimation mechanism for YSO jets, and the origin of their knots, are briefly examined.

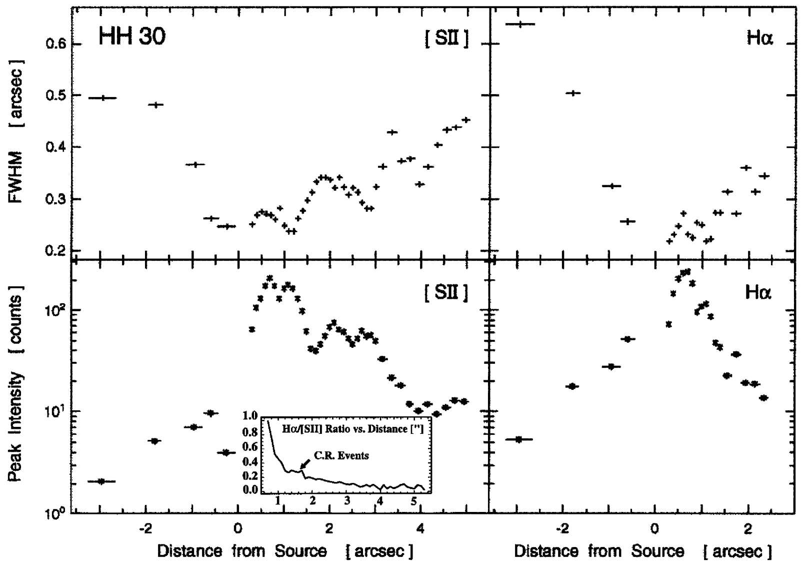

FIG. 2.—Plots of the HH 30 jet/counterjet [S II] and Hα intensity and width (FWHM in arcseconds) against distance from the source. For the elongated data points, in this and all subsequent plots, the horizontal width of the bar at a data point is a direct measure of the pixel binning used along the jet direction. Inset is a plot of the Hα/[S II] intensity ratio (normalized so that its peak is 1) for the first few arcseconds of the HH 30 jet. "C. R." marks the position of multiple cosmic ray events in the Hα images which could not be removed.

2. OBSERVATIONS AND RESULTS

Our images of the HL Tau region including HH 30 were obtained on 1995 March 6 using the Wide Field Planetary Camera 2 (WFPC2) aboard the *HST*. The standard [S II]λλ6716,6731(F673N), Hα (F656N), [O I]λ6300(F631N) filters along with a medium bandpass continuum (F547M) filter were used (for details, see Burrows 1995). Total on source integration times were 3 × 900 s, 2 × 1800 s, 2 × 900 s, and 2 × 500 s respectively. Here the first number indicates the actual number of exposures, as these were split to facilitate the removal of cosmic ray hits. The corrected optics of the WFPC2 has a point spread function (PSF) with an Airy disk diameter of 0".12 for λ = 555 nm. HL Tau itself was positioned on the f/28.3 Planetary Camera (PC) CCD PC1 with a pixel size of 0".0455 and HH 30 on the WF2 CCD of the f/12.9 Wide Field (WF) Camera. WF2 has a pixel size of 0".1 and thus undersamples the *HST* PSF. The WF *HST* Archive images of the HH 1 and HH 34 jets were taken on 1994 August 11 and 1994 September 16, respectively, using the [S II]λλ6716,6731 (F673N) filter and the total integration time in both cases was 3 × 1000 s. The HH 1 and HH 34 jets were positioned on the WF2 and WF4 CCDs, respectively. Data processing in all cases followed standard procedures (e.g., Stapelfeldt et al. 1995).

Figures 1*a*–1*e* (Plate L17) show our [S II], [S II]-F547M, Hα, [O I], and F547M images of HH 30. The [S II]-F547M continuum frame is virtually a "pure" emission line image obtained by subtracting the F547M continuum image from the [S II] frame after suitable scaling (see, e.g., Poetzel, Mundt, & Ray 1992). Comparison of Figures 1*a* and 1*c* show that the HH 30 jet is much more extensive in [S II] than Hα, a result that was already known from ground-based studies (Mundt et al. 1988). The wealth of detail in the *HST* data compared to the ground-based images is quite astonishing. For example, what constitutes the first knot of the HH 30 jet (hereafter knot A) in the ordinary ground-based image of MRBRS, and which upon deconvolution is resolved into two, is found to consist of at least seven subcondensations (A1–A7, see Fig. 1*f*). Both the jet and counterjet are observed to emerge perpendicular to two cusplike nebulae (see also Stapelfeldt 1996) which are most clearly seen in the continuum image of Figure 1*e*. Given that this flow is virtually in the plane of the sky (MRBRS), the dark lane between these nebulae is presumably the disk surrounding the HH 30 source. Major differences are observed in Figure 1 between the jet and the counterjet that cannot be explained by extinction effects. For example the Hα/[S II] ratio is much higher in the counterjet than in the jet, and the diameter of the counterjet appears broader at a given distance from the source (see also Figure 2).

In Figure 2 we present plots of the HH 30 jet/counterjet [S II] and Hα intensity and angular width (FWHM) against distance from the source. Here, and in all subsequent measurements of the jet diameter, we have fitted the lateral intensity profile of the jet with a Gaussian. It is immediately seen that the jet is well resolved laterally (FWHM ≥ 0".25) in both the [S II] and Hα images even close to the source, i.e., to within 0".3 or 42 AU assuming a distance of 140 pc to the Taurus Auriga Dark Cloud (Kenyon, Dobrzycka, & Hartmann 1994). Note that the Hα and [S II] jet widths were measured in the corresponding continuum subtracted frames, and that no correction for the *HST* PSF was applied. The latter correction is in any event small given the relatively large jet widths which are also, incidentally, well sampled by the WF CCD pixels. At 0".3 from the HH 30 source, the [S II] jet width (FWHM) ≈ 0".25. It is somewhat smaller in Hα at the same distance, and, generally speaking, the Hα widths are either close to or smaller than the corresponding [S II] widths over those portions of the jet where the two can be compared. The intensity of the jet is seen to decrease much more steeply in Hα than [S II]: more quantitatively, the drop in [S II] intensity is approximately fitted by a power law with $I[\mathrm{S\,II}] \propto L^{-1.9}$ whereas $I(\mathrm{H}\alpha) \propto L^{-2.4}$. At the same time the jet width is observed to slowly increase with increasing distance from the source such that the width of the jet (FWHM), W_j, can be approximated by

$$W_j = W_0 + \sin(\alpha) L, \qquad (1)$$

where $W_0 = 0''.23$, $\alpha = 0^\circ.85$, and L is measured in arcseconds. Thus, the opening angle of the jet beyond 0".25 from the

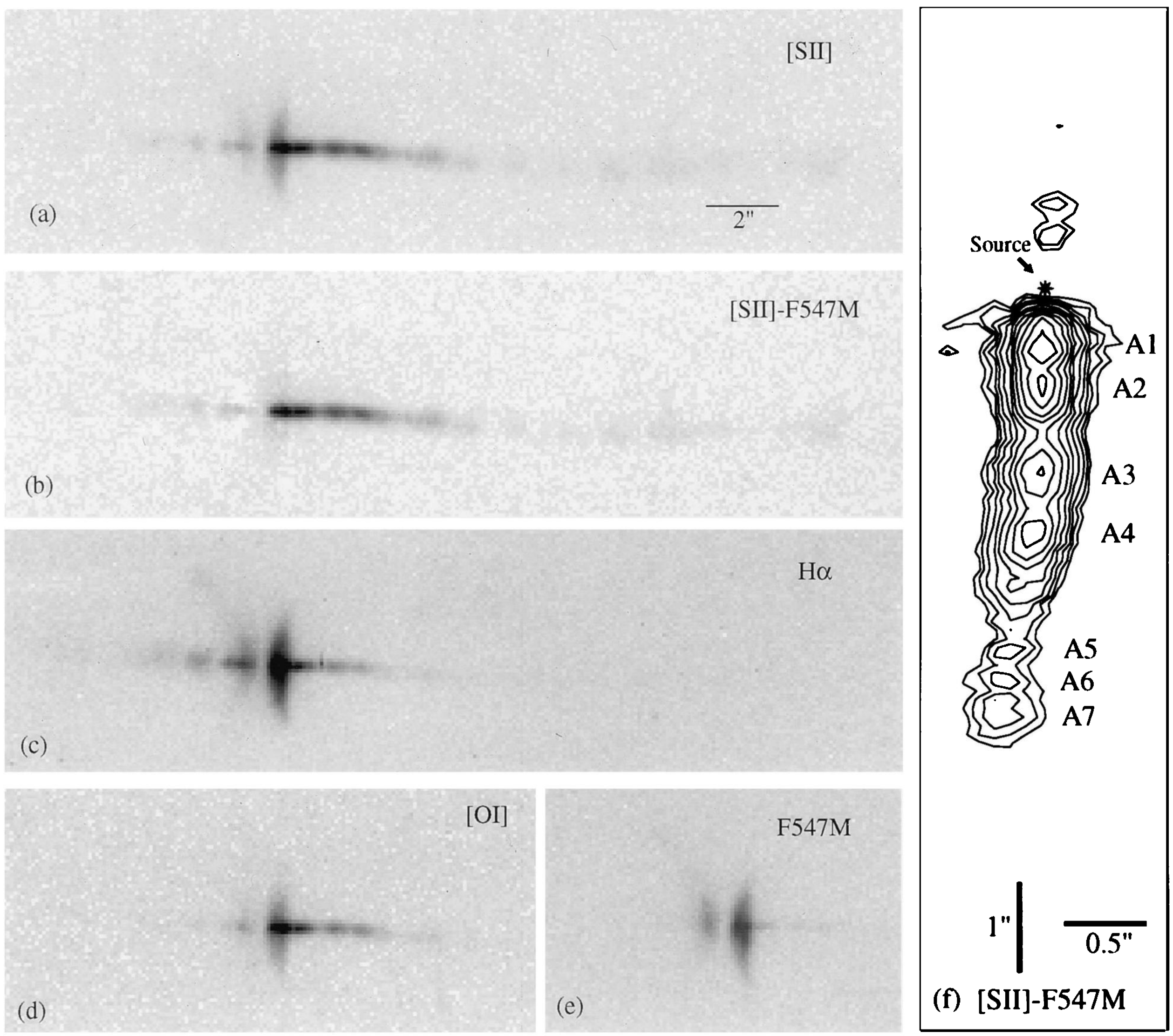

FIG. 1.—*HST* WFPC images of the HH 30 jet and counterjet in (*a*) [S II]λλ6716,6731, (*b*) [S II]λλ6716,6731-F547M, (*c*) Hα, (*d*) [O I]λ6300, and (*e*) F547M. The pure emission line frame (*b*) was made by subtracting the continuum image (*e*) from the [S II]λλ6716,6731 image as detailed in the text. (*f*) A contour plot of the first few arcseconds of the HH 30 jet and counterjet in [S II]λλ6716,6731 light after continuum (F547M) contraction. Note the large number of subcondensations A1–A7 found.

RAY et al. (see 468, L104)

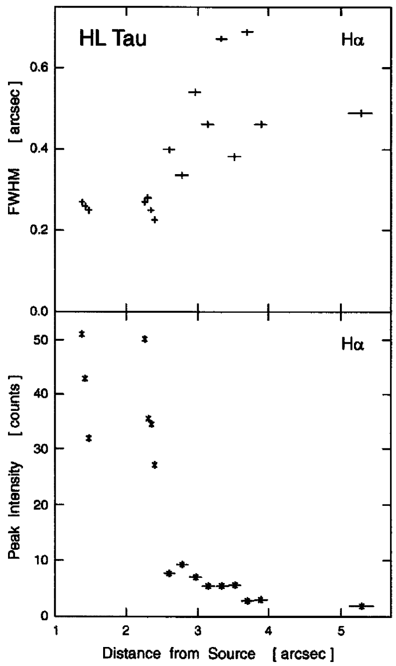

FIG. 4.—Plots of jet width (FWHM) and peak intensity (in counts) against distance from the source for the Hα emission of the HL Tau jet.

source is small, but the *actual jet width* is still very large at this distance. Assuming the jet has essentially zero angular width at the source, the initial full opening angle is thus also very large. It is at least 60° if one defines it in terms of the FWHM jet diameter and approximately a factor of 2 larger if the full width zero intensity (FWZI) diameter is used instead. Referring to Figures 2*a* and 2*b*, it should be noted that there may be an anticorrelation of the jet width with intensity in the sense that knots A2, A4, and A5 coincide with minima in the FWHM jet diameter. The anticorrelation is, however, not as clear-cut, as we shall see, as in the case of the HH 1 and HH 34 jets. A plot of the Hα/[S II] intensity ratio along the HH 30 jet is shown inset in Figure 2*c* where we have integrated laterally across the jet in both filters to minimize noise. Note that this ratio steadily declines with increasing distance from the source with no appreciable variations at the knots. Finally, we point out that the position of the source was assumed to be along the line connecting the jet and counterjet and midway between the two cusplike reflection nebulae. The dark lane separating the nebulae is at most 0″.3 wide along the outflow axis, so the error in the source position is certainly much less than 0″.15.

Turning now to HL Tau, in Figure 3 (Plate L18) we show a montage of six PC images of this star taken through [S II], Hα, [O I], and the F547M continuum filters along with the continuum subtracted [S II] and Hα images. Note that the continuum subtraction is not perfect in either case because of the steep color gradient across the HL Tau nebula (Stapelfeldt et al. 1995) and the unavoidable mismatch in continuum transmission properties of the emission line and F547M filters. In contrast to the HH 30 system, the HL Tau jet is quite difficult to see in all the emission line filters. This problem is exacerbated by the small pixel size of the PC CCD and, as we now know, the relatively large width of this jet close to the source (see Figure 4). Moreover, the contribution of the reflection nebula to the light through the narrowband filters is much more significant than is the case with HH 30, and, in fact, the jet itself is best seen in the continuum subtracted frames of Figures 3*e* and 3*f*. In Figure 3*e* we have marked the supposed position of HL Tau based on K band and 3.6 cm observations (Weintraub, Kastner, & Whitney 1995), and it can be seen that the projected jet (see Fig. 3*e*) passes close to these positions. No evidence for the counterjet observed on a larger scale (MRBRS) was observed by us on the PC images. Note also that the jet lies along the symmetry axis of the horseshoe-shaped reflection nebula recently discovered by Stapelfeldt et al. (1995) using WFPC2 and previously thought to be HL Tau itself. In Figure 4, we have plotted the FWHM width of the jet (in arcseconds) along with its relative peak intensity as measured through the Hα filter. The width is seen to decrease steeply as we get close to HL Tau (6″–3″) but closer again (around 1″.5) the width levels off to approximately 0″.25, or 40 AU at the distance of Taurus Auriga.

As stated in the introduction, we also reduced archive data on the HH 1 and HH 34 jets. In Figure 5 (Plate L19), we show our [S II] image of the HH 34 jet along with measurements of its [S II] width (FWHM) and [S II] intensity versus distance from the source. A similar image and plots are shown in Figure 6 (Plate L20) for the HH 1 jet. The source position for the HH 34 jet is based on an F850LP *HST* Archive continuum image not reproduced here. In determining the position of the HH 1 source (VLA-1) in the *HST* frames, we used the coordinates given by Rodríguez et al. (1990). When labeling the HH 34 knots (Fig. 5) we followed the nomenclature of Bührke et al. (1988), and in the case of HH 1 jet, those of Eislöffel et al. (1994) as far as possible.

For HH 34, it is clear even from examining the [S II] image in Figure 5, that the outer knots (I and J) are bow shaped; this is confirmed by the jet width versus distance plot in Figure 5 where the peaks and troughs in the width are found to coincide with what appears to be the tails and heads of the bow shocks respectively. Note also that the pattern of peaks and troughs is repeated at distances between 10″–15″ from the source even though from the [S II] image these inner knots (*E*–*I*) superficially do not resemble bow shocks. In this regard it is instructive to compare our results with those of Raga et al. (1991) who, using ground-based observations, derived similar values for the HH 34 jet width (≈0″.4 FWHM) at 4″–20″ from the source as found here. Rather interestingly, they also found the jet width to peak in the interknot regions but concluded that this was an effect of the non-Gaussian wings in the point-spread function (PSF) of their images. The current measurements now call into doubt whether the variations noted by Raga et al. (1991) were entirely attributable to a non-Gaussian PSF.

In Figure 6, a similar pattern of peaks and troughs for the width (FWHM) of the HH 1 jet is found, and again several knots (e.g., knot F_J) are suggestive of bow shocks. Finally, we mention that in both the case of HH 34 and HH 1, the jet width is at all times well resolved and for the HH 34 jet, it is still as large as 0″.25 (110 AU) at an angular distance of 0″.6 (270 AU) from the source. The HH 34 jet itself can be traced even closer to the source, but we refrain from quoting values for the jet width at such distances because of the increasing contribution of scattered light from the presence of a small conical reflection nebula.

3. DISCUSSION

From our analysis we find two important results. First, in those cases, i.e., HH 30 and HH 34, where we can trace the jet back very close to the source, the diameter of the jet remains large and decreases only slowly as the source is approached. Second, our analysis of the well-known knots in the HH 1 and

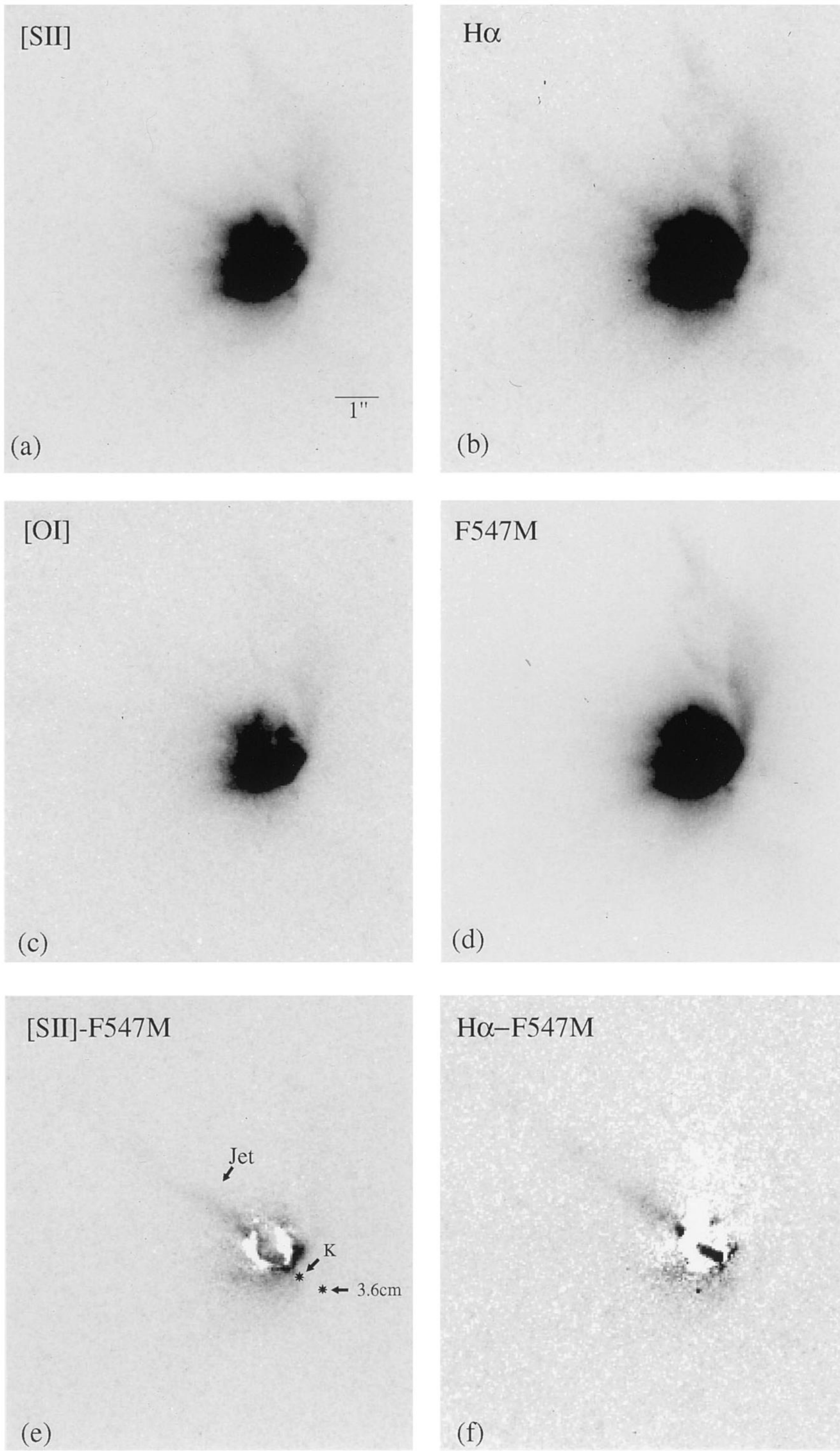

FIG. 3.—*HST* PC images of the HL Tau nebula and jet in (*a*) [S II]λλ6716,6731, (*b*) Hα, (*c*) [O I]λ6300 and (*d*) F547M, (*e*) [S II]λλ6716,6731-F547M, and (*f*) Hα-F547M. For details see text.

RAY et al. (see 468, L105)

1996ApJ...468L.103R

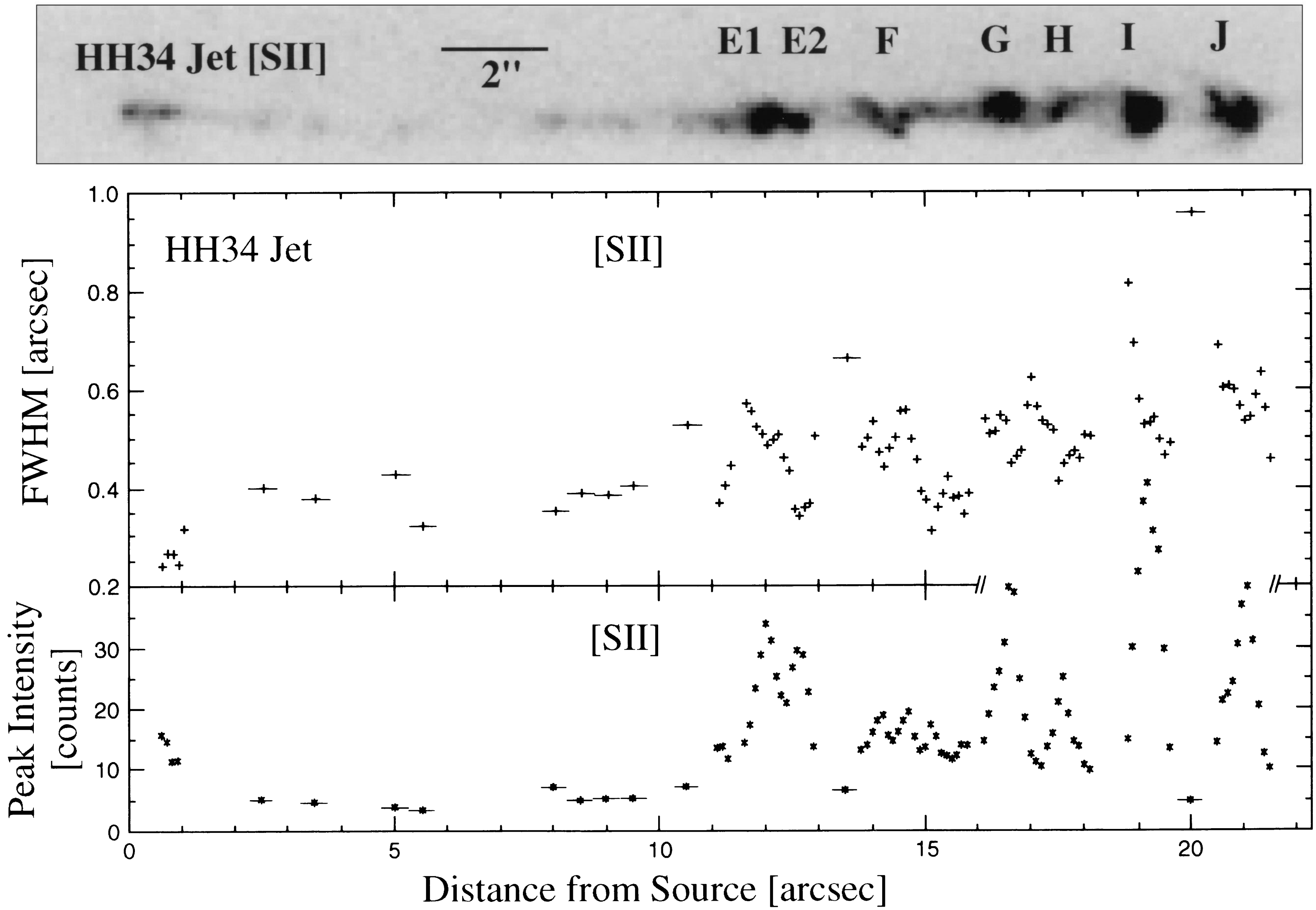

FIG. 5.—*Top*: our reduced *HST* Archive image of the HH 34 jet in [S II]λλ6716,6731 light with its source to the far-left. *Bottom*: plots of the jet width and peak intensity against distance from the HH 34 source using the [S II]λλ6716,6731 image. Note the broadening of the jet width *behind* the bright knots as expected from bow shocks.

RAY et al. (see 468, L105)

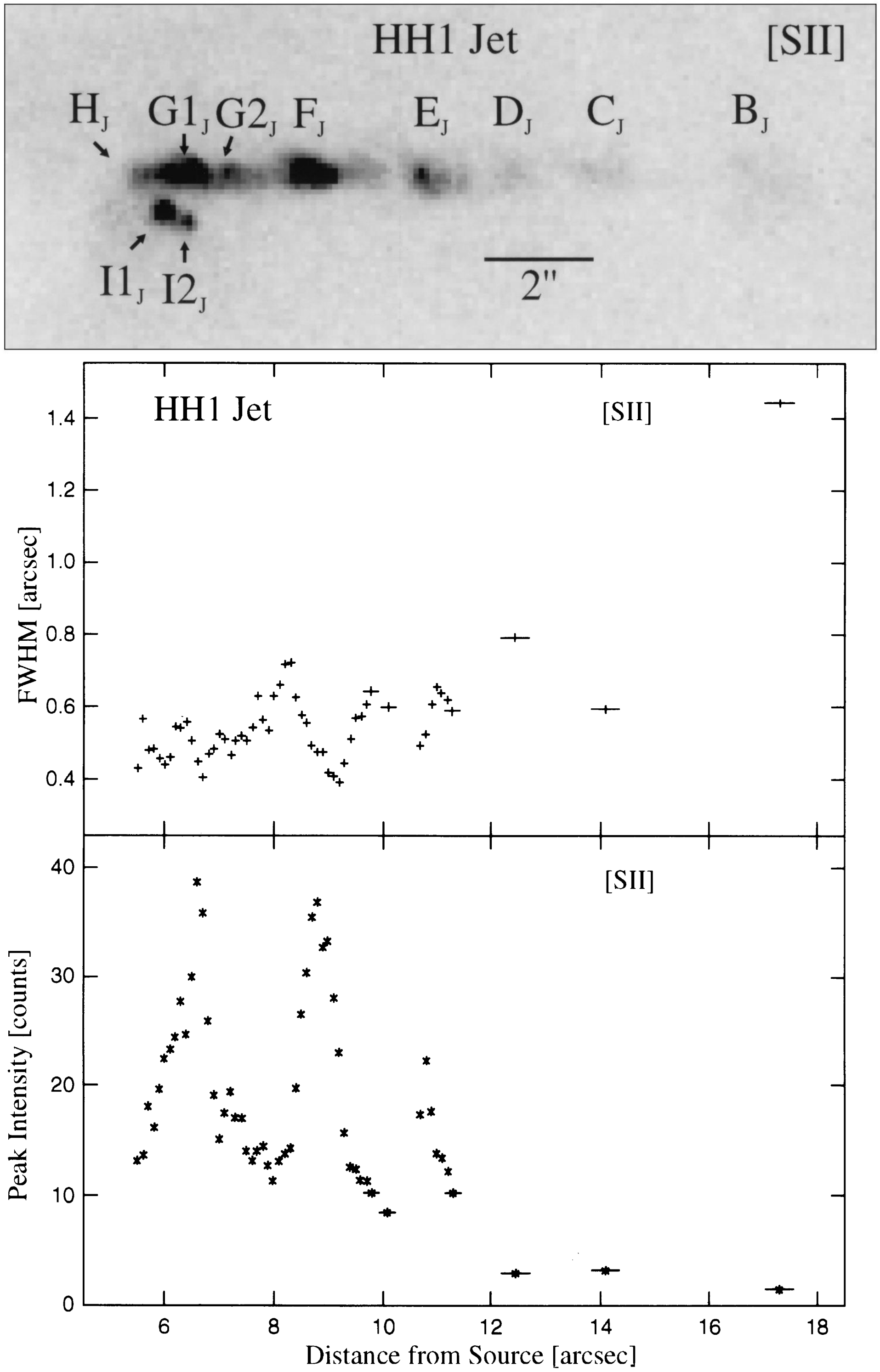

FIG. 6.—*Top*: our reduced *HST* Archive image of the HH 1 jet in [S II]λλ6716,6731 light. The VLA-1 source is outside the left boundary of the image at the distance indicated by the scale of the bottom plot. *Bottom*: plots of the jet width and peak intensity against distance from VLA-1 using the [S II]λλ6716,6731 image. As in the case of most of the bright knots in the HH 34 jet (see Fig. 5), the width and intensity vs. distance plots support the idea that most of these knots are bow shocks.

RAY et al. (see 468, L105)

HH 34 jets show that several of them morphologically resemble bow shocks. Thus, some of these knots appear to be "internal working surfaces," due to variations in the flow rather than the oblique crossing shocks as predicted by a number of models. Let us discuss these findings in more detail.

For both HH 30 and HH 34, the jet diameter (FWHM) asymptotically approaches ≈0″.2 close to the source. In HH 30 the strong obscuration caused by the circumstellar disk prevents us observing the jet closer to the source than about 0″.2–0″.3. For HH 34 scattered light from the small cometary-like reflection nebula also limits our ability to reliably measure diameters within 0″.5 from the source. In the case of the HL Tau jet, similar asymptotic behavior for its diameter as in the HH 30 and HH 34 jets is indicated, although here we are severely hampered by the scattered light and obscuration of the jet close to the star. Now, as mentioned in the previous section, it is usual to assume that the angular diameter of a YSO jet is effectively zero at its origin. The reason being that it very difficult theoretically to understand how one can launch a jet with velocities of a few hundred km s^{-1} without it originating from deep (i.e., ≲a few stellar radii) within the gravitational well of the parent star. If this is the case, then the inferred initial full opening angles of both the HH 30 jet/counterjet and HH 34 jets must be greater than 60° and 30°, respectively. It has to be emphasized that these estimates are lower bounds on two accounts: first, there is no reason to assume that the diameter of the jet drastically decreases just within the limits imposed on our analysis by the effects mentioned above. Second, as we have already stated, quoted opening angles are in a sense already underestimates since they are defined with respect to the diameter at FWHM as opposed to FWZI.

The above result is of fundamental importance to the theory of YSO jets. In particular it supports models in which YSO jets are initially poorly collimated winds close to the star which are then asymptotically collimated into "cylinders" with diameters of order a few tens of AU, e.g., Fendt et al. (1995) or Shu et al. (1995 and references therein). Finally, it is also worth pointing out that for those portions of the jet where the jet radius is large enough to measure from the ground, for example, in the case of the HH 1, HH 30, and HH 34 jets, we have found perfect agreement between the ground-based radius values and those derived from the *HST* data.

Turning now to the origin of the knots, our analysis of the HH 1 and HH 34 jets clearly shows that several of the knots are bow shocks. This appears to be in keeping with the "internal working surfaces" hypothesis. For HH 30 and HL Tau the situation is somewhat more complicated. The knots, for example, in the case of HH 30 do not display the same type of anticorrelation of width versus brightness as for the HH 1 and HH 34 jets. Morphologically there is no indication that the knots close to the source, nor for that matter those found at angular distances up to 3′ (e.g., MRBRS) look like bow shocks. Moreover the Hα/[S II] ratio plot for the knots in the HH 30 jet does not show any obvious change near the knots (apart from a slight decrease in the rate of decline of this ratio near knot A1) as might naively be expected if they were individual shocks. This contrasts with the case of the brightest knots in the HH 34 jet where the same ratio is found to vary with the individual knots (e.g., Raga et al. 1991). That is not to say that the internal working surfaces model does not predict a decay in the line intensities as a function of distance from the source, nor an increase in the [S II]/Hα ratio, at least in the analytic, asymptotic limit. Assuming that the variability of the outflow giving rise to the internal working surfaces is periodic, and using the steady, plane shock models of Hartigan, Raymond, & Hartmann (1987), one can show that the Raga & Kofman (1992) model predicts that the [S II] and Hα intensities should decrease with $L^{-1.1}$ and $L^{-3.8}$, respectively. As discussed in § 3, the corresponding exponents derived from our *HST* observations are −1.9 (for [S II]) and −2.4 (for Hα). It is not possible at this time to say whether this quantitative disagreement between the predictions from the analytic working surface model of Raga & Kofman (1992) and the observed decay of the line intensities with distance along the HH 30 jet is a result of the many simplifications of the model, or whether it implies that the knots along this jet are not internal working surfaces.

It would be interesting to test the line intensity with distance decay observed in the HH 30 jet with predictions from other knot production mechanisms, which unfortunately are not yet available. In particular Bacciotti, Chiuderi, & Oliva (1995) have put forward the idea that knots in YSO jets, or at least those closest to the source, are due to a series of (postshock) mild compressions rather than actual shocks. Their analysis suggests that the recombination timescale is close to the crossing time of the first visible portion of the jet, thus one would naturally expect the Hα/[S II] ratio to decline steadily, as is observed. The problem, however, with the idea of mild compressions is that, given the very high Mach numbers of these jets, it is difficult to imagine how compressions which give rise to such large increases in brightness *do not result in shocks*. One way around this difficulty might be to invoke the presence of very strong magnetic fields since the relevant Mach number then is not the standard thermal number but the magnetosonic Mach number, and this could be much smaller. Another possibility is that the knots in the HH 30 jet are due to density fluctuations in the outflow without concomitant changes in velocity; this scenario warrants further investigation.

T. R. and R. M. acknowledge funding from the German/Irish Science and Technology Cooperation Programme, and we would like to thank the referee, Frank Shu, for helpful comments.

REFERENCES

Bacciotti, F., Chiuderi, C., & Oliva, E. 1995, A&A, 296, 185
Bodo, G., Massaglia, S., Ferrari, A., & Trussoni, E. 1994, ApJ, 283, 655
Bührke, T., Mundt, R., & Ray, T. P. 1988, A&A, 200, 99
Burrows, C. J., ed. 1995, WFPC2 Instrument Handbook (Baltimore: STScI)
Edwards, S., Ray, T. P., & Mundt, R. 1993, in Protostars and Planets III, ed. E. Levy & J. Lunine (Univ. Arizona Press), 567
Eislöffel, J., & Mundt, R. 1992, A&A, 263, 292
Eislöffel, J., Mundt, R., & Böhm, K.-H., 1994, AJ, 108, 1042
Fendt, C., Camenzind, M., & Appl, S. 1995, A&A, 300, 791
Hartigan, P., Raymond, J., & Hartmann, L. 1987, ApJ, 316, 323
Kenyon, S. J., Dobrzycka, D., & Hartmann, L. 1994, AJ, 108, 1872
Mundt, R., Ray, T. P., & Bührke, T. 1988, ApJ, 333, L69
Mundt, R., Ray, T. P., Bührke, T., Raga, A. C., & Solf, J. 1990, A&A, 232, 37 (MRBRS)
Mundt, R., Ray, T. P., & Raga, A. C. 1991, A&A, 252, 740
Poetzel, R., Mundt, R., & Ray, T. P. 1992, A&A, 262, 229
Raga, A. C. 1995, Rev. Mexicana Astron. Astrofis. Ser. de Conf., 1, 103
Raga, A. C., & Kofman, L. 1992, ApJ, 386, 222
Raga, A. C., Mundt, R., & Ray, T. P. 1991, A&A, 252, 733
Rodríguez, L. F., Ho, P. T. P., Torrelles, J. M., Curiel, S., & Cantó, J. 1990, ApJ, 352, 645
Shu, F., Najita, J., Ostriker, E., & Shang, H. 1995, ApJ, 455, L155
Stapelfeldt, K. R. 1996, private communication
Stapelfeldt, K. R., et al. 1995, ApJ, 449, 888
Weintraub, D. A., Kastner, J. H., & Whitney, B. A. 1995, ApJ, 452, L141